

Thickness effect on superconducting properties of niobium films for radio-frequency cavity applications

Antonio Bianchi^{1,*} , Marco Bonura² , Carlota P A Carlos^{2,3}, Stewart Leith³, Guillaume Rosaz³ , Carmine Senatore⁴  and Walter Venturini Delsolaro³

¹ INFN, Milan, Italy

² Department of Quantum Matter Physics, University of Geneva, Geneva, Switzerland

³ CERN, Geneva, Switzerland

⁴ Department of Quantum Matter Physics and Department of Nuclear and Particle Physics, University of Geneva, Geneva, Switzerland

E-mail: antonio.bianchi@mi.infn.it

Received 3 April 2024, revised 31 May 2024

Accepted for publication 19 June 2024

Published 27 June 2024



Abstract

Niobium-coated copper radio-frequency cavities are cost-effective alternatives to bulk niobium cavities, given the lower material costs of copper substrates and their operation in liquid helium at around 4.2 K. However, these cavities historically exhibited a gradual degradation in performance with the accelerating field. This phenomenon, not yet fully understood, limits the application of niobium thin film cavities in accelerators where the real-estate gradient needs to be maximized. Recent studies on niobium films deposited on copper using high power impulse magnetron sputtering (HiPIMS) technique show promising results in mitigating the performance degradation of niobium thin film radio-frequency cavities.

This paper examines the effect of film thickness on the superconducting properties of niobium films deposited on copper using HiPIMS. The study provides insights into how the critical temperature, transition width, lower and upper critical fields, and critical current density vary with the film thickness. Increasing the thickness of niobium films deposited through HiPIMS is found to enhance superconducting properties and reduce densities of defects and structural irregularities in the crystalline lattice. This shows potential for enhancing overall performance and potentially mitigating the observed performance degradation in niobium thin film radio-frequency cavities. Additionally, the Ivry's scaling relation among critical temperature, thickness, and sheet resistance at the normal state appears applicable to niobium films up to approximately 4 μm . This extends the previously confirmed validity for niobium films, which was limited to around 300 nm thickness.

Keywords: niobium film, niobium-coated copper radio-frequency cavities, HiPIMS

* Author to whom any correspondence should be addressed.



Original Content from this work may be used under the terms of the [Creative Commons Attribution 4.0 licence](https://creativecommons.org/licenses/by/4.0/). Any further distribution of this work must maintain attribution to the author(s) and the title of the work, journal citation and DOI.

1. Introduction

Niobium films deposited on various substrates are currently being studied for several technological applications. These applications include detectors of single photons [1, 2], millimeter-wave receivers [3, 4], sub-millimeter-wave mixers [5, 6], and superconducting quantum interference devices (SQUIDs) [7, 8]. Niobium films are even employed in creating superconducting qubits for the advancement of quantum computers, relying on their elevated robustness and chemical stability [9, 10]. Furthermore, these niobium films find applications in constructing superconducting radio-frequency (SRF) cavities for particle accelerators.

Niobium-coated copper cavities were introduced in the early 1980s [11] as a promising alternative to bulk niobium cavities [12, 13]. One of the advantages of employing niobium thin film technology for SRF cavities lies in the cost reduction achieved by utilizing copper in place of niobium. This type of cavities was adopted at CERN for the Large Electron Positron collider (LEP-II) and, then, for the Large Hadron Collider (LHC). At INFN-LNL, niobium-coated copper cavities were employed for the Acceleratore Lineare Per Ioni (ALPI) machine. They were also utilized in various other accelerator facilities and projects, such as ELETTRA, SOLEIL, and SLS [12]. More recently, this technology was once again used for SRF cavities in the High Intensity and Energy Isotope Separator On Line Device (HIE-ISOLDE) linac at CERN.

The performance of SRF cavities is determined by the surface resistance of the superconductor present in their internal surface. At an operational temperature well below the superconducting transition temperature, the surface resistance R_s of a superconductor in the radio-frequency regime can be expressed as the sum of two terms: a temperature-dependent term, which depends on the fraction of unpaired carriers, and a second one, usually referred to as residual surface resistance. The residual surface resistance is typically associated with imperfections, interstitial impurities, and atomic size defects in the crystalline lattice [14, 15], as well as the trapped magnetic field during the cooling of cavities below the transition temperature from the normal to the superconducting state [16, 17]. Both terms of R_s depend on various parameters, as extensively discussed in the literature [14, 15, 18–20]. An in-depth discussion is not the subject of this paper; here, we only emphasize that the superconducting properties play a fundamental role in determining the surface resistance of a superconductor.

While niobium thin film cavities provide certain advantages, especially for large cavities operating at low frequencies [18], it is important to note that this type of cavities can exhibit serious performance degradation issues with increasing radio-frequency field [21–24], preventing their use in accelerators where the real-estate gradient needs to be maximized. This is the so-called Q -slope problem, which occurs due to the increase in the surface resistance of the niobium films when exposed to an increasing radio-frequency field, resulting in higher power dissipation. Recent studies have reported a significant reduction of the Q -slope phenomenon and the residual surface resistance in niobium films deposited on copper using

the high power impulse magnetron sputtering (HiPIMS) technique. Experimental results indicate that this coating technique allows for the growth of niobium thin films that exhibit surface resistance values comparable to those obtained on bulk niobium samples [25]. Using the HiPIMS deposition technique, promising results are also obtained in niobium thin film cavities at 400 MHz [26] and 1.3 GHz [13, 24] both at around 2 K and 4 K. To further improve the promising results obtained so far, we have investigated the effect of thickness on the superconducting properties of niobium films deposited on copper using HiPIMS.

The paper is organized as follows. Section 2 describes how the niobium films analyzed in this study are prepared and deposited on copper using the HiPIMS technique. In section 3, we present how we measure the superconducting properties of niobium films and investigate how these properties change with varying film thickness. In particular, the thickness effect on the critical temperature and the width of the transition from the superconducting state to the normal state is examined in section 3.1, whereas the influence of the film thickness on the lower and upper critical fields, as well as the critical current density, is explored in sections 3.2 and 3.3, respectively. Finally, conclusions are drawn in section 4.

2. Methods

Niobium films of various thicknesses are deposited on copper substrates using HiPIMS. During the deposition process, this technique enhances the production of niobium ions, which can be accelerated toward the substrate. When combined with a DC bias applied to the substrate, the energy of the impinging ions increases and their trajectory is redirected close to the substrate normal, thereby enhancing the densification of the growing thin film [27].

The samples of this study are made of OFE copper with a residual resistance ratio of approximately 50 and a thickness of 2 mm. Prior to coating, the copper slabs undergo a chemical polish with a mixture of sulfamic acid (H_3NSO_3 , 5 g L^{-1}), hydrogen peroxide (H_2O_2 , 5% vol.), n-butanol (5% vol.), and ammonium citrate (1 g L^{-1}) heated to 72°C for 20 minutes. After polishing, each substrate is rinsed with sulfamic acid to eliminate any native oxide buildup and is cleaned with de-ionized water and ultra-pure ethanol. Then, substrates are placed in an ultra-high vacuum stainless steel chamber, which is subsequently connected to the coating setup. This assembly is done in an ISO5 cleanroom. Afterwards, the system is brought outside the cleanroom and connected to the pumping group and gas injection lines. The vacuum chamber is pumped down to about 10^{-7} mbar. In addition, the pumping group and the entire coating system undergo a bakeout at 200°C for 48 hours. When the bakeout is completed, the vacuum chamber is maintained at 150°C until the coating process begins.

The HiPIMS deposition technique is detailed in previous works [25, 28, 29], including the coating setup specifically utilized for the samples analyzed in this study. The HiPIMS discharge is $200 \mu\text{s}$ long with a repetition frequency of 100 Hz

Table 1. Coating parameters for the niobium films deposited on copper using the HiPIMS technique. The table contains information on the sputtering gas, the pressure in the vacuum chamber during deposition, and the duration of the coating expressed in minutes. Moreover, the table includes values for the voltage and current associated with the DC bias and the plasma discharge. Finally, the temperature at which the sample is maintained for 48 hours post-deposition is specified. If the temperature is not specified in the table, the sample is cooled to room temperature after the coating process.

Sample	Sputtering parameters			DC bias		Plasma discharge		After coating
	Gas	Pressure (Pa)	Duration (min)	Voltage (V)	Current (A)	Voltage (V)	Current (A)	Temperature (°C)
R8-A2	Ar	0.23	180	-50	47	590	160	—
R8-D2	Ar	0.23	60	-50	47	590	160	—
R11-C2	Ar	0.26	240	-75	60	585	180	—
R16-A1	Kr	0.26	180	-75	50	625	162	200
R16-B2	Kr	0.26	120	-75	50	625	162	200
R16-C1	Kr	0.26	240	-75	50	625	162	200
R17-A1	Kr	0.27	240	-75	51	620	158	250
R17-C2	Kr	0.27	120	-75	51	620	158	250
R18-B1	Kr	0.24	120	-75	54	620	162	300
R18-C2	Kr	0.24	240	-75	54	620	162	300
R19-A1	Kr	0.22	240	-75	59	630	162	150
R19-B2	Kr	0.22	60	-75	59	630	162	150
R21-C2	Kr	0.34	240	-75	36	645	135	350

[28]. The coating temperature is monitored using an infrared thermal sensor and maintained constant at 150 °C with a fan [28]. A comprehensive summary of the coating parameters is provided in table 1. Depending on the sample, ultra-pure krypton or argon is introduced into the system until a pressure ranging from 2.2×10^{-3} mbar to 3.4×10^{-3} mbar is reached. The pressure during the coating of each sample is kept constant, while the duration of the deposition varies from 1 hour to 4 hours to achieve film thicknesses ranging from approximately $1 \mu\text{m}$ to $4 \mu\text{m}$, as the coating rate is around $1 \mu\text{m}$ per hour. However, this is a very rough estimate, as other coating parameters may also play a role. Similarly to the sputtering parameters, the voltage and current values of the plasma discharge and the DC bias to the substrate are specified for each sample in table 1. After the coating process, the samples are either maintained at a specific temperature for 48 hours, for post-coating annealing, or immediately cooled down to room temperature. The vacuum chamber is vented with dry air after this step.

Before measuring the superconducting properties, all samples are cut to dimensions of approximately $3 \times 3 \text{ mm}^2$ using electro-erosion. In addition, the thickness of each sample is measured by x-ray fluorescence via the attenuation method. Sample dimensions are essential for determining certain superconducting properties of the samples, as will be further explained in section 3.

3. Results and discussion

Superconducting properties of niobium films deposited on copper substrates are measured using a SQUID vibrating sample magnetometer (SQUID-VSM) [30]. The sample is vibrated at a known frequency and phase-sensitive detection is employed to enhance data collection speed and reject spurious signals. Unlike traditional VSMs, the signal generated by

a sample is not influenced by the frequency of vibration but is exclusively governed by the magnetic moment of the sample, the vibration amplitude, and the configuration of the SQUID detection circuit [30]. The setup includes a superconducting coil that can generate magnetic fields of up to 7 T, while also providing precise temperature control within the range of 1.8 K to 400 K. The external magnetic field is applied parallel to the plane of niobium films.

For all measurements presented in this study, the temperature sweep rate for determining the superconducting properties is kept constant at 1 K per minute throughout the data collection, whereas the field sweep rate for measuring the magnetization curve is kept equal to 10 mT s^{-1} . The sample undergoes a zero-field cooling prior to each measurement. Furthermore, to remove any residual magnetic flux potentially trapped in the superconducting coil, the coil is quenched before initiating the zero-field cooling of the sample.

Superconducting properties of samples are examined by measuring the magnetic moment of the samples at various values of temperature and applied magnetic field. More precisely, we measured the magnetic moment m of each sample for different values of the applied magnetic field from approximately 2.5 K up to about 12 K. The transition of the sample from the superconducting state to the normal state corresponds to a rather abrupt increase in the magnetic moment. The critical temperature and the transition width of each sample are determined by measuring the magnetic moment in the magnetometer as a function of temperature, with the application of an external magnetic field of 1.2 mT. This low magnetic field value is chosen to enable the measurement of these superconducting properties in the presence of an almost negligible magnetic field. As shown in figure 1, the onset of the change in the magnetic moment resulting from the transition of the sample from the superconducting state to the normal state is interpolated with a straight-line segment. Similarly, the magnetic

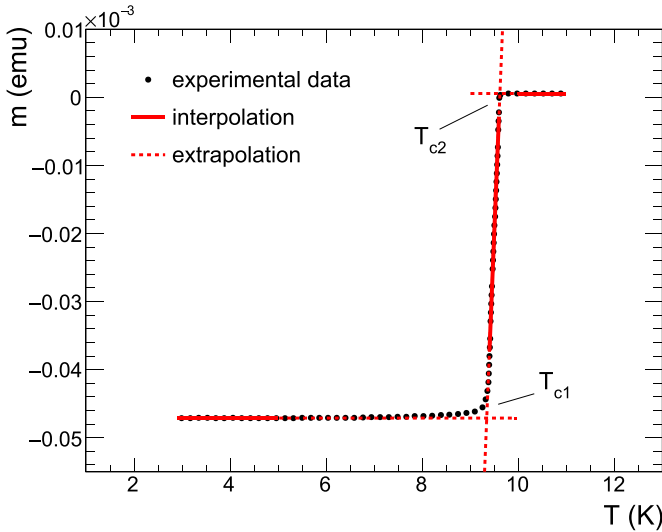


Figure 1. Magnetic moment (m) value of sample R11-C2 as a function of temperature (T) in the presence of an applied magnetic field of 1.2 mT. The interpolation of data in different temperature ranges is represented by solid lines, while the extrapolation of the fitted curves is displayed by dashed lines.

moment values from 2.5 K to 5 K and from 9.6 K to 11.5 K are interpolated with horizontal lines. By identifying the intersection point of the fitted curves as shown in figure 1, it is possible to determine the temperatures T_{c1} and T_{c2} that define the transition width of the sample from the superconducting state to the normal state. The value of critical temperature T_c is calculated by averaging the temperatures T_{c1} and T_{c2} , while the transition width ΔT_c is equal to the difference between T_{c1} and T_{c2} .

The magnetization curve of each sample is assessed at various temperatures approximately between -2 T and 2 T. The magnetic moment of each sample is measured as the external magnetic field is gradually increased from 0 T to 2 T, then reversed from 2 T to -2 T, and finally increased again from -2 T to 2 T. At the beginning of each magnetization curve measurement, the initial measurements of the magnetic moment as the applied magnetic field is progressively increased from the value of 0 T determine what is known as the virgin magnetization curve. The virgin magnetization curve initially exhibits a linear trend due to the perfect repulsion of the external magnetic field by the superconducting sample. Interpolating the virgin magnetization curve with a linear function enables the measurement of the entry field. Indeed, the entry field B_{entry} is identified when the magnetic moment starts to deviate from the initial linear behavior observed in the virgin magnetization curve. In this work, the entry field is defined as the applied magnetic field value where the discrepancy between the measured magnetic moment of the sample and the linear fit of the low-field data exceeds one standard deviation. The entry field is correlated with the lower critical field B_{c1} . In section 3.2, we make the assumption that B_{c1} equals B_{entry} solely for the purpose of evaluating the Ginzburg–Landau parameter of each sample. This assumption is valid in the absence of pinning and if no sample shape factors are involved. Some precautions have been taken to minimize

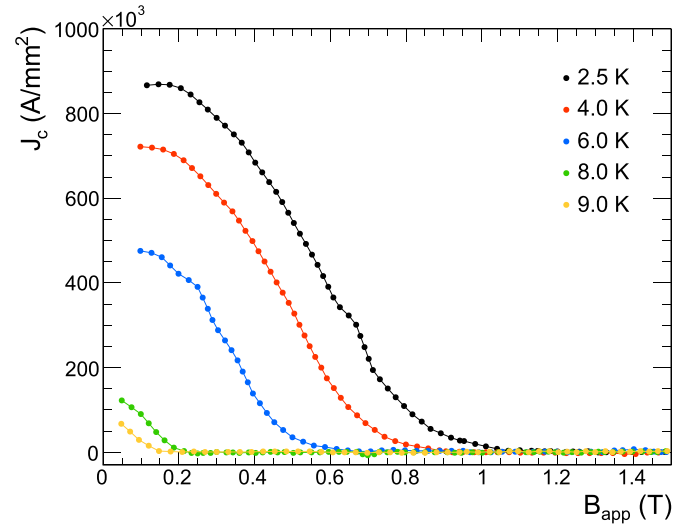


Figure 2. Critical current density (J_c) values of sample R11-C2 as a function of the applied magnetic field (B_{app}) at various temperatures.

potential limitations arising from our assumption. Each sample is cooled down in a zero-applied magnetic field before each measurement to minimize the pinning of the external magnetic field. In addition, we attempted to measure samples with approximately the same dimensions to minimize significant variations in the data due to their shape. Despite these precautions, a small discrepancy may still exist between B_{entry} and B_{c1} . Nevertheless, the determination of the Ginzburg–Landau parameter for our samples, where the value of B_{c1} plays a role as explained in section 3.2, spans the entire range of expected values reported in the literature. This confirms that the estimation of B_{c1} through the measurement of B_{entry} is not far from the actual value. More details are provided in section 3.2.

From the magnetization curves at various temperatures, we determined the temperature and magnetic field dependence of the critical current density J_c , using the Bean critical state model and applying the formula suitable for a slab geometry in the parallel magnetic field configuration [31, 32]:

$$J_c(T, B_{\text{app}}) = \frac{2\Delta m(T, B_{\text{app}})}{Vd} \quad (1)$$

where T is the temperature, B_{app} is the applied magnetic field, $\Delta m(T, B_{\text{app}})$ represents the separation between the two branches of the magnetic moment loop measured with opposite field sweep directions, V is the volume of the sample and d its thickness. Figure 2 shows the critical current density as a function of the applied magnetic field measured for a sample at various temperatures. For a fixed value of B_{app} , the lower the temperature, the higher the critical current density. We define B_{c2} as the field at which $J_c(T, B_{\text{app}})$ becomes zero.

Hereafter, we focus on the values of B_{c1} and B_{c2} estimated at 4 K, because niobium-coated copper cavities are primarily used at temperatures between 4.2 K and 4.5 K. Similarly, J_c values are assessed at 4 K and 200 mT. This specific field strength was chosen as it represents the minimum magnetic field at which the evaluation of J_c is feasible for the majority

Table 2. Superconducting properties of niobium films on copper analyzed in this study: T_c is the critical temperature, ΔT_c is the width of the transition from the superconducting state to the normal state, B_{entry} is the entry field at 4 K, and B_{c2} is the upper critical field at 4 K. J_c is the critical current density measured at 4 K and 200 mT. Moreover, the table includes the dimensions of each niobium film. The thickness of the niobium film is denoted as d . The width and length of each sample have a statistical error of 0.02 mm each.

Sample	d (μm)	Area (mm^2)	T_c (K)	ΔT_c (K)	B_{entry} (mT)	B_{c2} (T)	J_c (A mm^{-2})
R8-A2	3.51 ± 0.05	3.05×3.00	9.50 ± 0.01	0.24 ± 0.02	25 ± 1	1.20 ± 0.05	$(5.73 \pm 0.01) \times 10^4$
R8-D2	1.21 ± 0.04	3.10×2.95	9.39 ± 0.02	0.09 ± 0.03	12.5 ± 0.5	1.20 ± 0.05	$(1.26 \pm 0.01) \times 10^6$
R11-C2	3.54 ± 0.09	2.95×2.90	9.481 ± 0.002	0.027 ± 0.004	56 ± 1	0.95 ± 0.05	$(7.01 \pm 0.01) \times 10^5$
R16-A1	3.34 ± 0.08	3.05×2.95	9.453 ± 0.003	0.103 ± 0.006	19 ± 1	0.40 ± 0.05	$(6.58 \pm 0.01) \times 10^4$
R16-B2	2.24 ± 0.08	2.98×2.92	9.385 ± 0.005	0.12 ± 0.01	16 ± 1	1.35 ± 0.05	$(1.55 \pm 0.01) \times 10^5$
R16-C1	4.20 ± 0.11	2.96×2.96	9.463 ± 0.003	0.061 ± 0.006	19.5 ± 0.5	0.90 ± 0.05	$(6.95 \pm 0.01) \times 10^4$
R17-A1	3.82 ± 0.13	3.50×2.65	9.391 ± 0.002	0.102 ± 0.004	21 ± 1	0.75 ± 0.05	$(5.48 \pm 0.01) \times 10^4$
R17-C2	2.28 ± 0.08	3.20×3.10	9.38 ± 0.02	0.22 ± 0.04	21 ± 1	1.55 ± 0.05	$(9.73 \pm 0.01) \times 10^4$
R18-B1	2.39 ± 0.07	3.15×3.00	9.38 ± 0.03	0.11 ± 0.05	20 ± 1	1.30 ± 0.05	$(9.29 \pm 0.01) \times 10^4$
R18-C2	3.57 ± 0.11	3.00×2.65	9.40 ± 0.01	0.11 ± 0.02	12 ± 1	0.65 ± 0.05	$(5.74 \pm 0.01) \times 10^4$
R19-A1	3.89 ± 0.11	3.15×2.95	9.423 ± 0.006	0.09 ± 0.01	16 ± 1	0.70 ± 0.05	$(5.65 \pm 0.01) \times 10^4$
R19-B2	0.96 ± 0.03	3.00×2.95	9.363 ± 0.004	0.198 ± 0.007	12 ± 1	1.10 ± 0.05	$(5.50 \pm 0.01) \times 10^6$
R21-C2	4.15 ± 0.14	3.20×3.15	9.337 ± 0.003	0.128 ± 0.005	13 ± 1	0.70 ± 0.05	$(4.88 \pm 0.01) \times 10^4$

of the samples. Table 2 summarizes the superconducting properties of the niobium films on copper analyzed in this study. In particular, we report the values of B_{entry} , B_{c2} and J_c measured at 4 K, along with the values of T_c and ΔT_c measured in the presence of an almost negligible magnetic field. Additionally, the thickness and area of each sample are provided in the same table. In this work, only samples with a B_{entry} value at 4 K greater than or equal to 12 mT are considered, as those with lower values would not have significant practical applications in cavities. Indeed, radio-frequency cavities generally operate in the Meissner state, where the magnetic field is completely expelled from the superconductor that constitutes the cavities [33]. If we assume the value of 12 mT as the maximum peak magnetic field reached in a single-cell TESLA cavity at 1.3 GHz, it would correspond to an accelerating field of approximately 3 MV m^{-1} [34].

3.1. Critical temperature and transition width

The critical temperature of niobium films has been examined in relation to film thickness. In this work, the critical temperature of all samples, ranging from approximately 9.34 K to 9.5 K, is higher than that in bulk niobium [13, 21]. Figure 3(a) shows the values of critical temperature T_c as a function of film thickness d for all samples analyzed in this study. For most of the samples, the critical temperature falls between 9.34 K and 9.40 K, especially for those with a thickness lower than approximately $3 \mu\text{m}$. On the contrary, some samples thicker than $3 \mu\text{m}$ exhibit a critical temperature exceeding 9.40 K, reaching up to 100 mK higher. In further detail, the average critical temperature of all samples with a thickness below $3 \mu\text{m}$ is about 9.38 K, whereas those thicker than $3 \mu\text{m}$ present an average critical temperature higher by 50 mK. As already mentioned, the critical temperature of all niobium films analyzed in this study is slightly higher than the value in bulk niobium, which is approximately 9.25 K [35]. This has also been observed in different experiments on both samples [36, 37] and niobium-coated copper cavities [13, 21]. The

reason for this increase of T_c compared to the value measured in bulk niobium is not clear [36]. In some studies, this is attributed to the softening of the phonon spectrum in superconducting films, due to internal stress or strain in the lattice [21, 36–39].

Figure 3(b) shows the transition width ΔT_c as a function of the critical temperature T_c for all samples analyzed in this study. Except for one sample with a critical temperature of 9.50 K, which significantly deviates from the observed trend, there is a general decrease in transition width as the critical temperature increases. The minimum and maximum values of the transition width differ by approximately a factor of 8. ΔT_c is typically correlated with the quality of the niobium film. Higher sample quality results in a narrower transition width; conversely, films with lower quality generally present a broader transition [40–42].

3.2. Critical magnetic fields

In radio-frequency cavity applications, the penetration depth and coherence length of the superconducting material, from which the cavities are made, are important parameters that determine the cavity performance. The Ginzburg–Landau parameter k_{GL} is the ratio between the penetration depth λ and the coherence length ξ . This parameter is also correlated to B_{c1} and B_{c2} . Indeed, the greater the ratio between λ and ξ , the larger the ratio between B_{c2} and B_{c1} [43]. With the estimation of B_{c1} and B_{c2} , it becomes feasible to evaluate the Ginzburg–Landau parameter of each sample. In the limit of large λ/ξ values, the lower critical magnetic field B_{c1} can be approximated as follows [44]:

$$B_{c1} = \frac{\Phi_0}{4\pi\lambda^2} \ln(k_{\text{GL}}). \quad (2)$$

Conversely, the upper critical magnetic field B_{c2} is given by [44]:

$$B_{c2} = \frac{\Phi_0}{2\pi\xi^2} \quad (3)$$

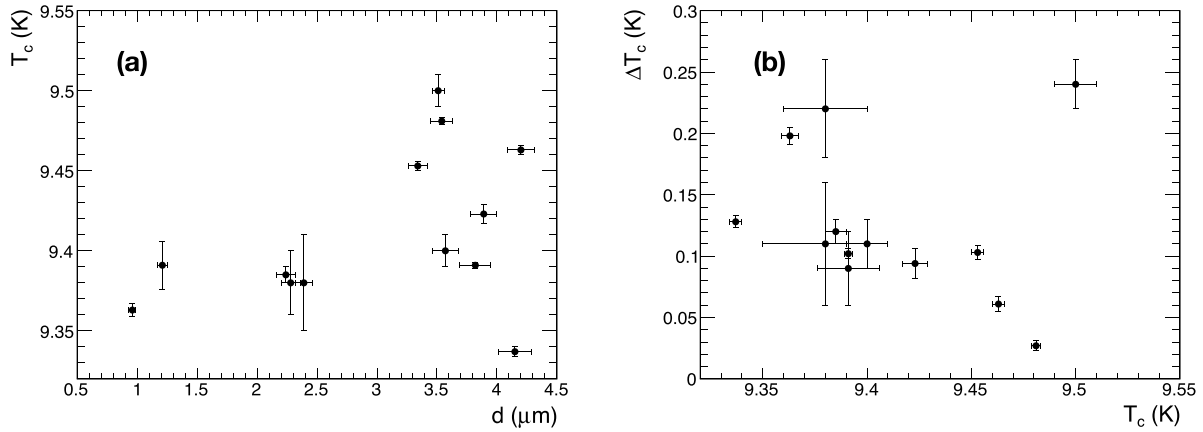


Figure 3. (a) Dependence of the critical temperature (T_c) values on the film thickness (d) for niobium films on copper analyzed in this study. (b) Dependence of the transition width (ΔT_c) on the critical temperature.

Therefore, the ratio between B_{c2} and B_{c1} can be expressed as:

$$\frac{B_{c2}}{B_{c1}} = 2k_{\text{GL}}^2 \frac{1}{\ln(k_{\text{GL}})}. \quad (4)$$

By obtaining the real solution of equation (4), the parameter k_{GL} can be determined. As explained in section 3, B_{c1} has been assumed to be equal to B_{entry} for estimating k_{GL} , although small discrepancies may be present despite precautions taken to minimize them. Another limitation arises because equation (4) is based on the assumption of large λ/ξ values, which could potentially lead to uncertainties in the estimation of k_{GL} , especially for niobium films with k_{GL} values close to those of bulk niobium. Nevertheless, the k_{GL} values of our samples span almost the entire range expected for niobium films used in thin film radio-frequency cavity applications [45]. Figure 4(a) shows the Ginzburg–Landau parameter of all samples at 4 K as a function of the film thickness. Since the values of B_{entry} and B_{c2} listed in table 2 refer to a temperature of 4 K, k_{GL} is the Ginzburg–Landau parameter evaluated at 4 K. Our niobium films demonstrate k_{GL} values within the range of 3 to 11, while k_{GL} values of niobium films for superconducting cavities typically vary from 3.5 to 12 [45]. Obtaining k_{GL} values within the expected range enables us to have confidence in the Ginzburg–Landau parameter determination procedure employed in this work. Minor deviations from the actual value, resulting from assuming B_{c1} equal to B_{entry} and the partial fulfillment of the large λ/ξ limit in some samples, have negligible implications for the scope of this study. As shown in figure 4(a), a correlation between the Ginzburg–Landau parameter and the film thickness has been observed. In particular, the Ginzburg–Landau parameter generally tends to decrease with increasing film thickness. This may suggest that increasing the thickness of the niobium film on a copper cavity leads to lower values of surface resistance. It is worth mentioning that two samples, with a thickness of approximately 3.4 μm , exhibit a k_{GL} value of around 3, which is quite close to the lower limit of the expected range in niobium films for radio-frequency cavities. This does not appear to be correlated with different coating parameters when compared to all other samples in the study.

Furthermore, one sample was produced using argon, and the other using krypton.

In the dirty limit, the coherence length as a function of temperature can be expressed as [46]:

$$\xi(T) = 0.852 \sqrt{\xi_0 l} \frac{1}{\sqrt{1 - \frac{T}{T_c}}} \quad (5)$$

where l is the mean free path and ξ_0 is the BCS coherence length, which is 38 nm in niobium [43]. By substituting the expression of the coherence length into equation (3), one obtains the mean free path l of each sample:

$$l = \frac{\Phi_0}{2\pi B_{c2}} \frac{1}{(0.852)^2 \xi_0} \left(1 - \frac{T}{T_c}\right) \quad (6)$$

where T is assumed to be equal to 4 K as B_{c2} is evaluated at that temperature. Figure 4(b) shows the values of the mean free path as a function of the film thickness. The values of l , which span from ~ 4 nm to ~ 17 nm for the samples analyzed in this study, are very close to the expected range where the surface resistance of niobium thin film cavities exhibits a minimum [18, 21]. The dirty limit assumption may not be entirely satisfied, as the values of l in our samples are smaller than ξ_0 only by a factor ranging from 2 to 9, whereas the dirty limit condition requires that the value of l be significantly smaller than ξ_0 [46]. Once the mean free path is known, the residual resistivity ratio (RRR) can be calculated as follows: $\text{RRR} = l/2.55$, where l is expressed in nanometers [47]. Some authors use the value 2.7 instead of 2.55 for niobium [22].

Ivry *et al* discovered a universal relation among the critical temperature, the film thickness, and the sheet resistance of the film at the normal state (R_n) [48]. This relation has been demonstrated to be valid for various superconducting materials across a wide range of thicknesses (approximately from 1 nm to 1 μm) [48]:

$$dT_c = AR_n^{-B} \quad (7)$$

where A and B are fitting parameters. Ivry's relation is valid for superconducting films deposited on any substrates. In accordance with the convention adopted in the original paper [48],

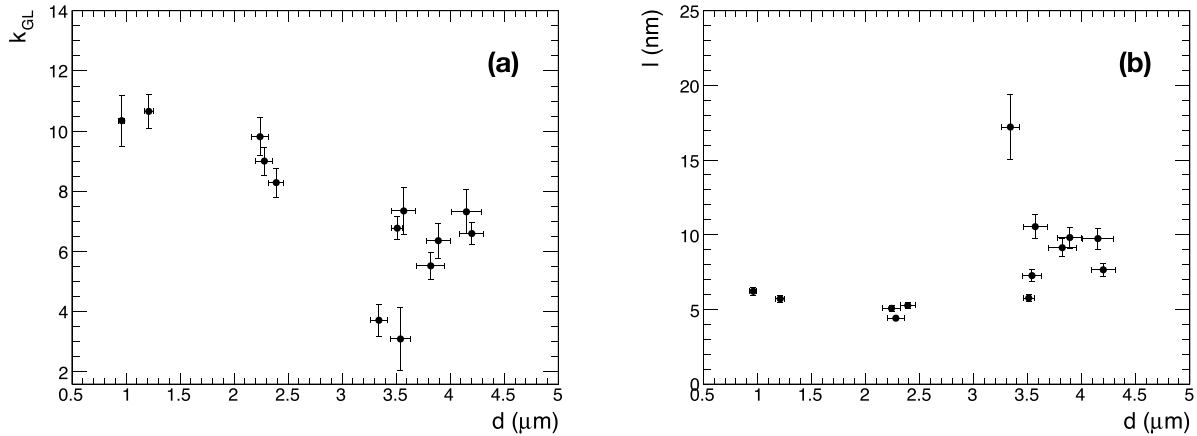


Figure 4. (a) Dependence of the Ginzburg–Landau parameter (k_{GL}) on the film thickness (d). (b) Thickness dependence of the mean free path (l).

d , T_c and R_n are considered unitless when the values provided are in nanometers, Kelvin, and ohms per square, respectively. Similarly, A and B are hereafter considered dimensionless. We have used Ivry's relation to validate our mean free path estimation for the samples analyzed in this work. Indeed, although the sheet resistance of our films in the normal state has not been directly measured, it can be estimated using the relation between electrical resistivity ρ_0 and mean free path:

$$\rho_0 l = \text{constant} \quad (8)$$

where the material constant of niobium is $3.72 \times 10^{-6} \mu\Omega \text{ cm}^2$ [49]. As a consequence, R_n is equal to ρ_0/d . To verify the scaling relation in niobium, Ivry *et al* utilized data from Gubin *et al* [36], which covered niobium films with thicknesses ranging from 7 nm to 300 nm. They found that A is equal to 611.38 and B is equal to 0.761 in niobium films [48]. More recently, Pinto *et al* [40] found in a different dataset that the parameters A and B are 1350 ± 120 and 0.76 ± 0.05 , respectively. The fitting parameter B is in excellent agreement in both studies, while the parameter A in Pinto's study is larger than that in Ivry's. Figure 5 shows the two different trends derived from their respective datasets. Additional data from the datasets of Gershenson *et al* [50] and Quateman [51] appear to mainly follow the trend recently found by Pinto *et al*. Similarly, our data primarily follow the same trend observed in the datasets from Pinto, Gershenson, and Quateman, as shown in figure 5. This suggests that the derivation of the mean free path for niobium films analyzed in this work is reasonably satisfactory, even if the dirty limit assumption is not fully met in some samples. In addition, the relation among d , T_c , and R_n found by Ivry *et al* appears to be valid not only for niobium films with a thickness lower than 300 nm but also within the range of ~ 1 to $\sim 4 \mu\text{m}$, which corresponds to the range of our samples.

Another method to estimate the Ginzburg–Landau parameter for each sample is presented by Ooi *et al* [47]. Using the mean free path evaluated for each sample, it is possible to calculate the corresponding Ginzburg–Landau parameter.

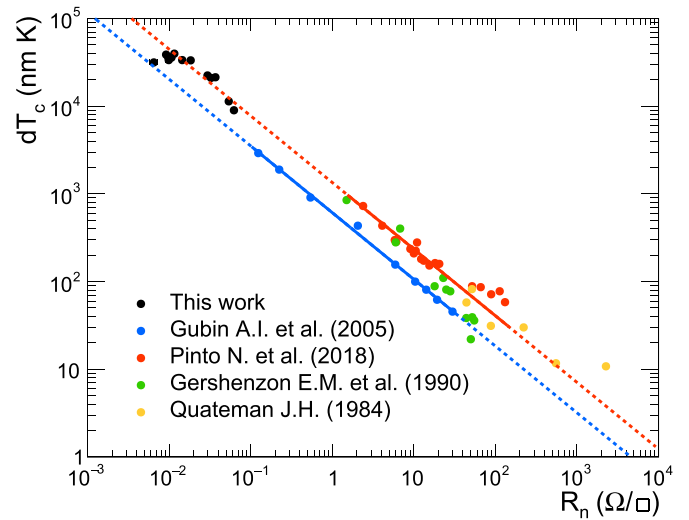


Figure 5. Dependence of the product of the film thickness (d) and the critical temperature (T_c) on the sheet resistance at the normal state (R_n) for niobium films. Data from various datasets are reported: in blue, the data by Gubin *et al* [36], in red, the data by Pinto *et al* [40], in green and yellow, those by Gershenson *et al* [50] and Quateman [51], respectively. Data in black corresponds to this study. In addition, the two trends derived by Ivry *et al* [48] from the data of Gubin *et al* and by Pinto *et al* from their own data are shown. The solid lines correspond to the interpolation range, while the dashed lines indicate the extrapolation of the observed trends.

From the values of the mean free path illustrated in figure 4(b), we obtain Ginzburg–Landau parameters in substantial agreement with the values shown in figure 4(a), except for the two samples approximately $1 \mu\text{m}$ thick, whose Ginzburg–Landau parameters are reduced by around 30%. For the calculation, we used a Ginzburg–Landau parameter of 1.26 for pure niobium at 4 K, as previously measured in niobium samples with high purity [52, 53]. The Ginzburg–Landau parameters obtained from the mean free path fall within the expected range of values for niobium films for superconducting cavity applications.

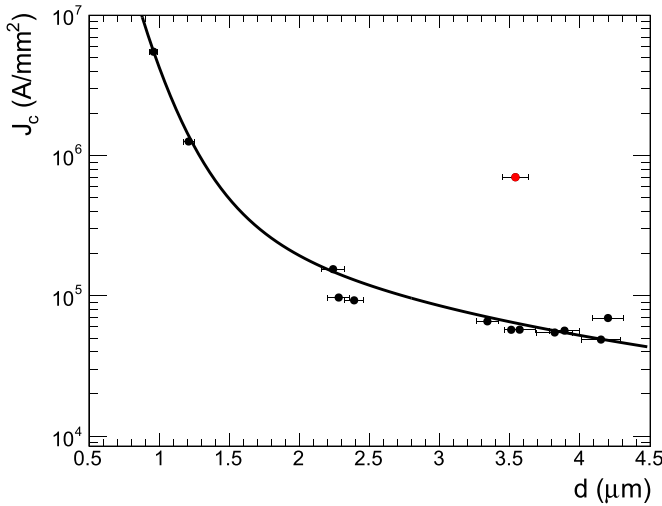


Figure 6. Values of critical current density (J_c) at 4 K and 200 mT as a function of the film thickness (d). Except for the sample in red which significantly deviates from the observed trend, the data are interpolated from the sum of two power functions.

3.3. Critical current density

The critical current density J_c can be significantly enhanced through the creation of pinning centers that effectively anchor fluxons against the Lorentz force acting on them. These pinning centers are created within the crystalline lattice and can result from material impurities, dislocations, grain boundaries, and precipitates with sizes of the order of the coherence length [32, 54]. For example, it is well-known that metallurgical processes, such as cold working or heat treatment, typically increase the density of pinning centers and, as a result, enhance the critical current density in type-II superconductors [32]. This is also applicable to niobium, where the critical current density can provide insights into the presence of structural defects within the crystalline lattice [13, 55, 56]. In this study, the critical current density of niobium films has been determined using the Bean critical state model in a slab geometry under the influence of a parallel magnetic field. The values of J_c at 4 K and 200 mT for all films are provided in table 2, while the thickness dependence of these values is presented in figure 6.

Except for one data point that significantly deviates from the observed trend, the data in figure 6 are interpolated from the following function:

$$J_c = (3.8 \pm 0.7) \times d^{-(6.8 \pm 0.8)} + (0.50 \pm 0.08) \times d^{-(1.6 \pm 0.1)} \quad (9)$$

where J_c and d are given in MA mm^{-2} and μm , respectively. The decrease in J_c values with increasing film thickness indicates a progressive reduction in the density of defects and structural irregularities in the crystalline lattice as the film thickness increases. A niobium film with a thickness of $4 \mu\text{m}$ exhibits a critical current density of approximately $5 \times 10^4 \text{ A mm}^{-2}$. However, this value is still higher than that of bulk niobium. Based on the interpolation of J_c , a thickness of $11 \mu\text{m}$ results in a J_c value of 10^4 A mm^{-2} , which is two orders of magnitude

higher compared to that of niobium ingots used in the production of bulk niobium radio-frequency cavities [54].

Along with surface resistance and kinetic inductance, the depairing current density J_d is one of the most relevant physical quantities for modern superconducting devices [57]. In SRF cavities, J_d determines the maximum current that these devices can support [20, 58]. In superconductors in the dirty limit, J_d is directly proportional to the thermodynamic critical field, which is the ultimate performance limit of SRF cavities [45]. Using BCS theory, J_d can be calculated at any given temperature [57]. In the dirty limit, the normalization factor J_{s0} is defined by the equation $J_{s0} = B_{c0}/(\mu_0 \lambda_0)$, where B_{c0} is the thermodynamic critical field at 0 K, λ_0 is the London penetration depth at 0 K, and μ_0 is the magnetic permeability. Depending on the specific values of B_{c0} and λ_0 , which can vary slightly [21, 35, 45, 59, 60], we generally obtain a value of J_{s0} from 5 to 8 MA mm^{-2} for niobium. Assuming an idealized BCS superconductor with a Dynes gamma factor of 0, J_d at 4 K can be approximated to $0.5 \times J_{s0}$ [57]. It is worth mentioning that the critical current density of the thinnest films analyzed in this study approaches the depairing current density at 4 K, which is the theoretical limit.

4. Conclusion

The purpose of this study is to understand how the superconducting properties of niobium films deposited on copper using HiPIMS vary with changing film thickness. The HiPIMS coating technique has demonstrated promising results in mitigating the Q -slope and reducing the residual surface resistance in niobium-coated copper radio-frequency cavities. Therefore, it holds the potential for successful application in the production of cavities for upcoming particle accelerators.

In this study, we analyzed the superconducting properties of niobium films with thicknesses ranging from approximately $1 \mu\text{m}$ to $4 \mu\text{m}$. The results presented here indicate that both the critical temperature and the Ginzburg–Landau parameter, calculated from the ratio between the lower and upper critical magnetic fields, show a correlation with the film thickness. In general, a high critical temperature and a small Ginzburg–Landau parameter contribute to reducing the surface resistance of superconductors in the radio-frequency regime. In the pursuit of optimizing the surface resistance of niobium films for radio-frequency cavity applications, increasing the film thickness appears to align with this objective. Indeed, thicker niobium films, analyzed in this study, exhibit a higher critical temperature and a smaller Ginzburg–Landau parameter. Moreover, both transition width and critical current density decrease with increasing thickness; therefore, the quality of the films appears to improve, while the presence of defects and structural irregularities within the crystalline lattice seems to decrease, which is desirable for radio-frequency cavity applications. Finally, in this study, we assessed the mean free path of our samples in the dirty limit based on the experimental measurements of the upper critical magnetic field. The obtained values of the mean free path are in quite close proximity to the expected value where the surface resistance of niobium thin

film radio-frequency cavities exhibits a minimum. Using the mean free path estimation in our samples, the scaling relation among critical temperature, thickness, and sheet resistance at the normal state, as discovered in superconducting films by Ivry *et al* appears applicable to niobium films up to approximately 4 μm . This extends the previously confirmed validity for niobium films, which was limited to around 300 nm thickness.

Based on our findings, thicker niobium films deposited on copper using the HiPIMS technique demonstrate improved superconducting properties and reduced densities of defects and structural irregularities in the crystalline lattice. Consequently, these improvements hold promise for enhancing overall performance and potentially mitigating the Q -slope observed in niobium thin film radio-frequency cavities. Nevertheless, finding a compromise between film thickness and structural aspects in cavities is essential. This involves addressing concerns like the potential detachment of the film from the substrate, which is more likely with thicker films, mechanical issues caused by differing thermal contractions between niobium films and copper substrates, and ensuring uniform coating of films with an adequate thickness across extensive areas.

Data availability statement

All data that support the findings of this study are included within the article (and any supplementary files).

Acknowledgments

The authors would like to thank Dr Dorothea Fonnesu and Dr Akira Miyazaki for useful discussion. The research leading to this work is part of the Future Circular Collider study.

ORCID iDs

Antonio Bianchi  <https://orcid.org/0000-0003-0343-7497>
 Marco Bonura  <https://orcid.org/0000-0002-8512-0989>
 Guillaume Rosaz  <https://orcid.org/0000-0001-5987-128X>
 Carmine Senatore  <https://orcid.org/0000-0002-9191-5016>

References

- [1] Semenov A, Engel A, Il'in K, Gol'tsman G, Siegel M and Hübers H-W 2003 Ultimate performance of a superconducting quantum detector *Eur. Phys. J. Appl. Phys.* **21** 171
- [2] Friedrich S 2008 Superconducting tunnel junction photon detectors: theory and applications *J. Low Temp. Phys.* **151** 277
- [3] Jia H and Mansour R R 2019 Millimeter-wave ultra wideband multilayer superconducting filter *IEEE Trans. Appl. Supercond.* **29** 1
- [4] Anischenko S, Larkin S Y and Khabayev P 1993 Microwave receiver system with quantum superconducting Josephson junctions based on LTSC and HTSC *Int. J. Infrared Millim. Waves* **14** 665
- [5] Karasik B, Gaidis M, McGrath W, Bumble B and LeDuc H 1997 Low noise in a diffusion-cooled hot-electron mixer at 2.5 THz *Appl. Phys. Lett.* **71** 1567
- [6] Dierichs M, Panhuyzen R, Honingh C, De Boer M and Klapwijk T 1993 Submicron niobium junctions for submillimeter-wave mixers using optical lithography *Appl. Phys. Lett.* **62** 774
- [7] Fujimaki N, Gotoh K, Imamura T and Hasuo S 1992 Thermal-noise-limited performance in single-chip superconducting quantum interference devices *J. Appl. Phys.* **71** 6182
- [8] Bouchiat V, Faucher M, Thirion C, Wernsdorfer W, Fournier T and Pannetier B 2001 Josephson junctions and superconducting quantum interference devices made by local oxidation of niobium ultrathin films *Appl. Phys. Lett.* **79** 123
- [9] Lisenfeld J, Lukashenko A, Ansmann M, Martinis J and Ustinov A 2007 Temperature dependence of coherent oscillations in Josephson phase qubits *Phys. Rev. Lett.* **99** 170504
- [10] Bennett D A, Longobardi L, Patel V, Chen W and Lukens J E 2007 RF-SQUID qubit readout using a fast flux pulse *Supercond. Sci. Technol.* **20** S445
- [11] Benvenuti C, Circelli N and Hauer M 1984 Niobium films for superconducting accelerating cavities *Appl. Phys. Lett.* **45** 583
- [12] Calatroni S 2006 20 years of experience with the Nb/Cu technology for superconducting cavities and perspectives for future developments *Physica C* **441** 95-101
- [13] Venturini Delsolaro W *et al* 2023 Progress and R/D challenges for FCC-ee SRF *EPJ Tech. Instrum.* **10** 1
- [14] Padamsee H 2009 *RF Superconductivity: Science, Technology and Applications* (Wiley)
- [15] Valente-Feliciano A-M 2016 Superconducting RF materials other than bulk niobium: a review *Supercond. Sci. Technol.* **29** 113002
- [16] Romanenko A, Grassellino A, Crawford A, Sergatskov D and Melnychuk O 2014 Ultra-high quality factors in superconducting niobium cavities in ambient magnetic fields up to 190 mG *Appl. Phys. Lett.* **105** 234103
- [17] Huang S, Kubo T and Geng R 2016 Dependence of trapped-flux-induced surface resistance of a large-grain Nb superconducting radio-frequency cavity on spatial temperature gradient during cooldown through T_c *Phys. Rev. Accel. Beams* **19** 082001
- [18] Bonin B 1996 Materials for superconducting cavities, *CERN Accel. Sch.* 191-200
- [19] Gurevich A and Kubo T 2017 Surface impedance and optimum surface resistance of a superconductor with an imperfect surface *Phys. Rev. B* **96** 184515
- [20] Kubo T 2022 Effects of nonmagnetic impurities and subgap states on the kinetic inductance, complex conductivity, quality factor and depairing current density *Phys. Rev. Appl.* **17** 014018
- [21] Benvenuti C, Calatroni S, Campisi I, Darriulat P, Peck M, Russo R and Valente A-M 1999 Study of the surface resistance of superconducting niobium films at 1.5 GHz *Physica C* **316** 153
- [22] Aull S, Junginger T, Knobloch J, Sublet A, Valente-Feliciano A-M, Venturini Delsolaro W and Zhang P 2015 On the understanding of Q-slope of niobium thin films *17th Int. Conf. on RF Superconductivity* (<https://doi.org/10.18429/JACoW-SRF2015-TUBA03>)
- [23] Miyazaki A and Venturini Delsolaro W 2019 Two different origins of the Q-slope problem in superconducting niobium film cavities for a heavy ion accelerator at CERN *Phys. Rev. Accel. Beams* **22** 073101
- [24] Vega Cid L, Atieh S, Bellini G, Bianchi A, Ferreira L, Leith S, Pereira Carlos C, Rosaz G and Venturini Delsolaro W 2023

- Results of the R&D RF testing campaign of 1.3 GHz Nb/Cu cavities *21st Int. Conf. on RF Superconductivity (SRF23)* (JACoW Publishing) pp 621–6
- [25] Arzeo M, Avino F, Pfeiffer S, Rosaz G, Taborelli M, Vega Cid L and Venturini Delsolaro W 2022 Enhanced radio-frequency performance of niobium films on copper substrates deposited by high power impulse magnetron sputtering *Supercond. Sci. Technol.* **35** 054008
- [26] Pereira Carlos C 2023 Nb coatings from 1.3 GHz to 400 MHz *FCC week 2023*
- [27] Avino F, Fonnesu D, Koettig T, Bonura M, Senatore C, Fontenla A P, Sublet A and Taborelli M 2020 Improved film density for coatings at grazing angle of incidence in high power impulse magnetron sputtering with positive pulse *Thin Solid Films* **706** 138058
- [28] Rosaz G, Bartkowska A, Carlos C P, Richard T and Taborelli M 2022 Niobium thin film thickness profile tailoring on complex shape substrates using unbalanced biased high power impulse magnetron sputtering *Surf. Coat. Technol.* **436** 128306
- [29] Wang C Y, Pereira C, Leith S, Rosaz G and Anlage S M 2023 Microscopic examination of SRF-quality Nb films through local nonlinear microwave response (arXiv:2305.07746)
- [30] Quantum Design, Magnetic property measurement system: MPMS 3 2010 User's Manual 1500-100F1
- [31] Bean C P 1964 Magnetization of high-field superconductors *Rev. Mod. Phys.* **36** 31
- [32] Iwasa Y 2009 *Case Studies in Superconducting Magnets: Design and Operational Issues* (Springer Science Business Media)
- [33] Posen S, Valles N and Liepe M 2015 Radio frequency magnetic field limits of Nb and Nb₃Sn *Phys. Rev. Lett.* **115** 047001
- [34] Yamamoto A 2009 Superconducting RF cavity development for the International Linear Collider *IEEE Trans. Appl. Supercond.* **19** 1387
- [35] Finnemore D, Stromberg T and Swenson C 1966 Superconducting properties of high-purity niobium *Phys. Rev.* **149** 231
- [36] Gubin A, Il'in K, Vitusevich S, Siegel M and Klein N 2005 Dependence of magnetic penetration depth on the thickness of superconducting Nb thin films *Phys. Rev. B* **72** 064503
- [37] Choi J, Kim Y-K, Kim C-D, Kim S and Jo Y 2020 Enhancing the critical temperature of strained niobium films *Mater. Res. Express* **7** 076001
- [38] Amos R, Breyer P, Huang H and Lichtenberger A 1995 Stress and source conditions of DC magnetron sputtered Nb films *IEEE Trans. Appl. Supercond.* **5** 2326
- [39] Strongin M, Kammerer O, Crow J, Parks R, Douglass D and Jensen M 1968 Enhanced superconductivity in layered metallic films *Phys. Rev. Lett.* **21** 1320
- [40] Pinto N, Rezvani S J, Perali A, Flammia L, Milošević M V, Fretto M, Cassiogo C and De Leo N 2018 Dimensional crossover and incipient quantum size effects in superconducting niobium nanofilms *Sci. Rep.* **8** 4710
- [41] Fonnesu D, Baris A, Calatroni S, Amador L L, Pfeiffer S, Rosaz G, Bonura M and Senatore C 2022 Reverse coating technique for the production of Nb thin films on copper for superconducting radio-frequency applications *Supercond. Sci. Technol.* **35** 125003
- [42] Russo R 2007 Quality measurement of niobium thin films for Nb/Cu superconducting RF cavities *Meas. Sci. Technol.* **18** 2299
- [43] Kittel C 2005 *Introduction to Solid State Physics* (Wiley)
- [44] Tinkham M 2004 *Introduction to Superconductivity* (Courier Corporation)
- [45] Padamsee H, Knobloch J and Hays T 2009 *RF Superconductivity for Accelerators* (Wiley)
- [46] Orlando T, McNiff E Jr and Beasley M 1979 Critical fields, Pauli paramagnetic limiting and material parameters of Nb₃Sn and V₃Si *Phys. Rev. B* **19** 4545
- [47] Ooi S, Tachiki M, Konomi T, Kubo T, Kikuchi A, Arisawa S, Ito H and Umemori K 2021 Observation of intermediate mixed state in high-purity cavity-grade Nb by magneto-optical imaging *Phys. Rev. B* **104** 064504
- [48] Ivry Y, Kim C-S, Dane A E, De Fazio D, McCaughan A N, Sunter K A, Zhao Q and Berggren K K 2014 Universal scaling of the critical temperature for thin films near the superconducting-to-insulating transition *Phys. Rev. B* **90** 214515
- [49] Mayadas A, Laibowitz R and Cuomo J 1972 Electrical characteristics of RF-sputtered single-crystal niobium films *J. Appl. Phys.* **43** 1287
- [50] Gershenson E, Gershenson M, Gol'tsman G, Lyul'kin A, Semenov A and Sergeev A 1990 Electron-phonon interaction in ultrathin Nb films *Sov. Phys. JETP* **70** 505 (available at: www.jetp.ras.ru/cgi-bin/dn/e_070_03_0505.pdf)
- [51] Quateman J 1986 T_c suppression and critical fields in thin superconducting Nb films *Phys. Rev. B* **34** 1948
- [52] French R 1968 Intrinsic type-2 superconductivity in pure niobium *Cryogenics* **8** 301
- [53] Saito K 2003 Theoretical critical field in RF application 11th Workshop on RF Superconductivity
- [54] Dhavale A S, Dhakal P, Polyanskii A A and Ciovati G 2012 Flux pinning characteristics in cylindrical niobium samples used for superconducting radio frequency cavity fabrication *Supercond. Sci. Technol.* **25** 065014
- [55] Tedmon C, Rose R and Wulff J 1965 Resistive measurements of structural effects in superconducting niobium *J. Appl. Phys.* **36** 829
- [56] Antoine C 2019 Influence of crystalline structure on RF dissipation in superconducting niobium *Phys. Rev. Accel. Beams* **22** 034801
- [57] Kubo T 2020 Superfluid flow in disordered superconductors with dynes pair-breaking scattering: Depairing current, kinetic inductance and superheating field *Phys. Rev. Res.* **2** 033203
- [58] Maki K 1963 On persistent currents in a superconducting alloy. I *Prog. Theor. Phys.* **29** 10
- [59] Halbritter J 1974 On surface resistance of superconductors *Zeitschrift für Physik* **266** 209
- [60] Maxfield B W and McLean W 1965 Superconducting penetration depth of niobium *Phys. Rev.* **139** A1515